Order online now!

www.rockland.com
tech@rockland.com
+1 484.791.3823

Datasheet for 212-901-D84

Neurofilament M Antibody

Overview

Description:	Anti-Neurofilament M (Chicken) Antibody - 212-901-D84
Item No.:	212-901-D84
Size:	100 µL
Applications:	IF, WB, IHC
Reactivity:	Human, Mouse, Rat, Bovine, Chicken
Host Species:	Chicken

Product Details

Background:	NF-M antibody detects Neurofilament M protein. Neurofilaments are the 10nm or intermediate filament proteins found specifically in neurons, and are composed predominantly of three major proteins called NF-L, NF-M and NF-H. NF-M is the neurofilament middle or medium molecular weight polypeptide and runs on SDS-PAGE gels at 145-160 kDa, with some variability across species boundaries. Antibodies to NF-M are useful for identifying neuronal cells and their processes in tissue sections and in tissue culture. NF-M antibodies can also be useful to visualize neurofilament accumulations seen in many neurological diseases, such as Amyotrophic Lateral Sclerosis (Lou Gehrig's disease) and Alzheimer's disease. Neurofilament M Antibody is ideal for investigators involved in Cell Signaling and Neuroscience research.
Synonyms:	chicken anti-Neurofilament M antibody, Neurofilament medium polypeptide, NF-M, 160 kDa neurofilament protein, Neurofilament 3, Neurofilament triplet M protein
Host Species:	Chicken
Clonality:	Polyclonal
Format:	IgY

Target Details

Gene Name:	Nefm
Reactivity:	Human, Mouse, Rat, Bovine, Chicken
Immunogen Type:	Recombinant Protein

Immunogen:	Anti-NF-M Monoclonal Antibody was produced by repeated immunizations with recombinant C-terminus part of NF-M expressed in E. coli.
Purity/Specificity:	Anti-NF-M antibody is directed against NF-M protein. The antibody is a total IgY fraction. Expect reactivity with the following species based on sequence homology: chicken, human, mouse. Cross reactivity with NF-M from other species has not been determined.
Relevant Links:	• UniProtKB - P12839 • GeneID - 24588 • UniProtKB - P12839.4

Application Details

Tested Applications:	IF, WB
Suggested Applications:	IHC (Based on references)
Application Note:	Anti- Neurofilament M antibody is tested for use in Western Blotting and IF. Specific . Expect a band of approximately 145 kDa in size corresponding to NF-M proteins in the appropriate cell lysate or extract. Researchers should determine optimal titers for applications that are not stated below.
Assay Dilutions:	All assays should be optimized by the user. Recommended dilutions (if any) may be listed below.
IF:	1:1000
WB:	1:5000

Formulation

Physical State:	Liquid
Concentration:	10 MiniBlots titrated reagent Sufficient to run approximately 10 miniblots
Buffer:	0.02 M Potassium Phosphate, 0.15 M Sodium Chloride, pH 7.2
Preservative:	0.01% (w/v) Sodium Azide

Shipping & Handling

Shipping Condition:	Dry Ice
Storage Condition:	Store vial at -20° C prior to opening. This product is stable at 4° C as an undiluted liquid. For extended storage, aliquot contents and freeze at -20° C or below. Avoid cycles of freezing and thawing. Dilute only prior to immediate use.

Expiration: Expiration date is one (1) year from date of receipt.

Images

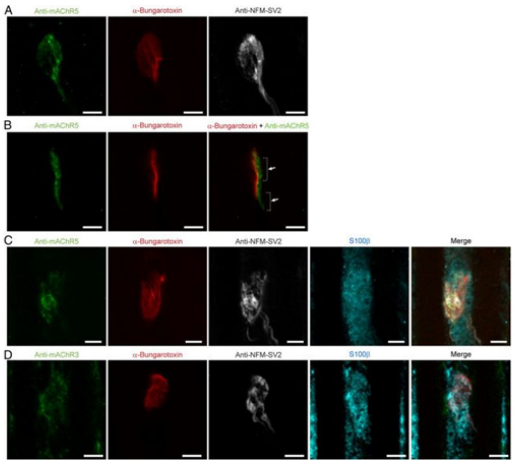

Immunofluorescence Microscopy
Type 5 and Type 3 mAChRs at poly-innervated NMJs. A, False color confocal z-stack of 10 images of immunohistochemical labeling of Type 5 mAChRs (mAChR5; green), postsynaptic nAChRs (α-bungarotoxin; red), and presynaptic terminals (NF-SV2; gray) at a P7 poly-innervated NMJ. Note the diffuse organization of mAChR5 that covers most of the endplate area in red. B, A single focal plane of the NMJ presented in A showing mAChR5 (green) and postsynaptic nAChRs (red). Note that mAChR5 and nAChR were located at a different level and did not colocalize (hyphenated lines and arrows show 2 regions where mAChR5 and nAChR did not overlap). C, False color confocal z-stack of 5 images of quadruple immunohistochemical labeling of another P7 poly-innervated NMJ showing the diffuse distribution of mAChR5 (green), postsynaptic nAChRs (α-bungarotoxin; red), presynaptic terminals (NF -SV2; gray), and PSCs (S100β; cyan). D, False color confocal z-stack of 5 images of quadruple immunohistochemical labeling of another P7 poly-innervated NMJ showing the distribution mAChR3. As for mAChR5, mAChR3 labeling was diffuse and uniform throughout the endplate area (red). Scale bars, 5 µm. Fig 8.
PMID: 23345206

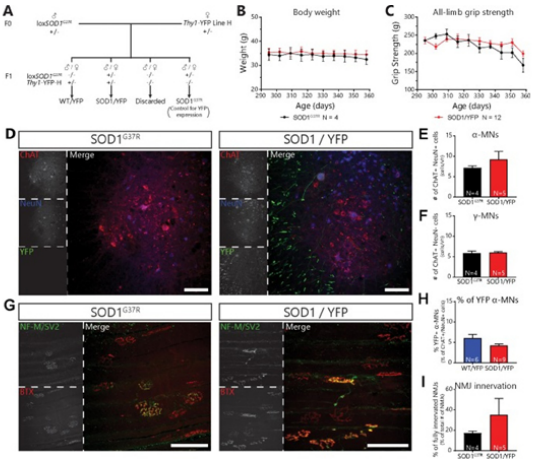

Immunofluorescence Microscopy

(A) Mating scheme for SOD1G37R/YFP and WT/YFP mice. (B) Body weight curve of SOD1G37R and SOD1G37R/YFP mice (black and red, respectively), showing a similar weight between both groups (repeated measures two-way ANOVA; Effect of genotype: p=0.7059; Effect of time: p=0.1237; Interaction: p=0.8874). (C) All-limb grip strength curve of SOD1G37R and SOD1G37R/YFP mice (black and red respectively), showing a parallel grip strength loss between both groups (repeated measure two-way ANOVA; Effect of genotype: p=0.3186; Effect of time: p<0.0001; Interaction: p=0.2189). (D) Representative example of lumbar spinal cord sections from SOD1G37R (left) and SOD1G37R/YFP (right) mice at P360 (Red: ChAT; Blue: NeuN; Green: YFP). Note the presence of YFP-positive neuronal cell bodies and projecting axons (in the white matter) in SOD1G37R/YFP mice. (E) (F) Quantification of the number of α-MNs (E) ChAT + NeuN + cells) and γ-MNs (F) ChAT + NeuN cells) per ventral horn at P360, showing that SOD1G37R/YFP and SOD1G37R mice had similar levels of α-MN loss (unpaired t-test; p=0.3648) and that γ-MNs were unaffected (unpaired t-test; p=0.8624). (H) Percentage of YFP-expressing α-MNs in WT/YFP and SOD1G37R/YFP mice, illustrating that, although the proportion of YFP-expressing MNs tended to be lower in SOD1 G37R /YFP mice, the difference was not statistically significant (Mann-Withney test; p=0.1447). (G) Representative images of NMJs in the Tibialis anterior muscle of SOD1G37R (left) and SOD1G37R/YFP mice (right) at P360 (Red: α-BTX; Green: NF-M and SV2). (I) Quantification of the percentage of fully innervated NMJs in the Tibialis anterior at P360, demonstrating that SOD1G37R/YFP and SOD1G37R mice had similar levels of denervation (GLM effect of genotype: p=0.214; post-test; p=0.316). The number of replicates for each experiment are indicated in the figure directly for clarity. Animals were sex-matched and age-matched between groups for each experiment. Data presented as mean ± SEM. The raw values for graphs in panels (B) (C) (E) (F) (H) and (I) are presented in Figure 2- Supplement – Source data one with the full results of the statistical tests for (B) and (C). Scale bars: 100 µm. Fig 2.

PMID: 30320556

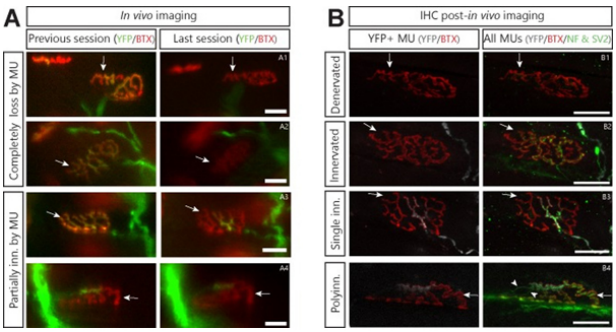

Immunofluorescence Microscopy

(A) and (B) illustrate the same NMJ during in vivo and after IHC respectively. Arrows point to a distinctive landmark of postsynaptic area. (A). Examples of NMJs that were asynchronously lost by the imaged MU (A1 and A2), partially lost by the MU (A3) or partially innervated by the MU for several weeks (A4). Green: YFP-labeled axon; Red: nAChR labeled with BTX. Note the slight change in the appearance of A1 and A2 is due to a change in the imaging angle (tilting) due to variable leg placement. This is also notable by the apparent change in distance between the NMJ of interest and another nearby NMJ. (B). Confocal images of the same NMJs as in A after immunolabeling for the presynaptic markers NF-M and SV2. Note how vacated postsynaptic sites in A2 and A4 were innervated by another, YFP-negative, motor axon, while those in A1 and A3 were not. The stable partial innervation by the imaged MU in A4 was thus likely due to lasting polyinnervation (B4, arrowhead). Green: NF-M and SV2 (all MUs); Gray: YFP-labeled axon; Red: nAChR labeled with BTX. Note how distinctive parts of the 'pretzel' shape of postsynaptic receptors is identical between the in vivo the post-in vivo confocal image. Importantly, the main axonal branch visible in A4 is not visible in B4 as it was at a lower focal plane which was not included in the confocal stack shown in B4. Scale bars: 25 µm. Figure 4—figure supplement 2

PMID: 30320556

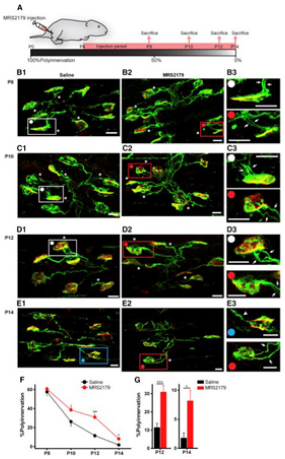

Immunofluorescence Microscopy

(A) Schematic representation of subcutaneous MRS2179 injection. Daily subcutaneous injections of 40 µM MRS2179 were performed next to the soleus muscle from P4 to P14. Mice were scarified at P8, P10, P12, and P14.
(B–E) Confocal images presenting examples of saline-injected (first column, B1–E1) and MRS2179-injected soleus (second column, B2–E2), labeled to observe presynaptic nerve terminals (stained with antibodies against NF-M and SV2, green) and postsynaptic endplates (nAChRs stained with α-bungarotoxin, red). Note that more polyinnervated NMJs (asterisks) were present in MRS2179-injected mice at all ages. The state of polyinnervation was defined by the number of independent nerve terminals that innervate the same endplate. B3–E3 (third column) show a higher magnification of polyinnervated NMJs, highlighted by a rectangle in B1 and B2 to E1 and E2. Independent inputs (green) innervating the same endplate area (red) are indicated by white arrows. White squares and dots represent the enlarged region from saline-injected mice, whereas red square and dots represent the enlarged region from MRS2179-injected mice. Note that most P14 saline-injected mice (E1 and E3, blue square and dot) were mono-innervated by a single input, marked by a white arrowhead.
(F) Diagram showing the time course of synapse elimination in saline-injected (black) compared with MRS2179-injected (red) mice at P8 (Nsaline = 8, NMRS = 8), P10 (Nsaline = 8, NMRS = 8), P12 (Nsaline = 7, NMRS = 7), and P14 (Nsaline = 7, NMRS = 6). Note that MRS2179-injected mice had a delay in synapse elimination, highlighted by the presence of more polyinnervated NMJs at P12 and P14.
(G) Histograms highlighting the difference in the percentage of polyinnervation between saline-injected (black) and MRS2179-injected (red) mice at P12 and P14.
p < 0.05; p ≤ 0.001. Scale bars, 10 µm. Fig 6.
PMID: 30463006

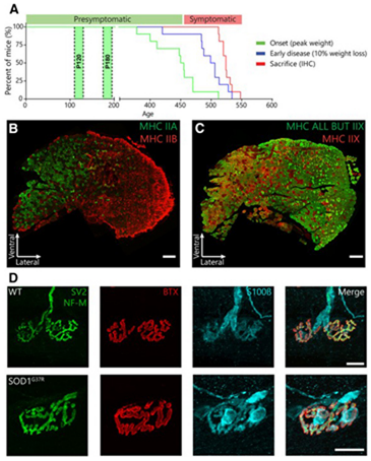

Immunofluorescence Microscopy
Disease progression in SOD1G37R mice and fiber type composition of the STM muscle. A, Kaplan–Meier plot of the ages at which disease onset (green; median age: 456 d) and early disease (blue; median age: 506 d) are reached in SOD1G37R mice under our conditions. All the symptomatic animals displayed similar motor phenotypes and were killed (red, median 527 d) after the early disease stage. Experiments on presymptomatic animals were carried at P120 and P180. B, C, Immunostaining of STM cross-sections for MHC Type IIb (FF, red) and IIa (FR, green; B) or all isotypes except IIx (all but IIx, green) and Type IIx (FF, red; C). Scale bars = 200 µm. D, Representative examples of presynaptic nerve terminals (green, SV2 and NF-M), postsynaptic nAChRs red (α-BTX), and glia (blue; S100β) labeling from the STM of P120 WT and SOD1G37R mice. Scale bars = 20 µm. Fig 1. PMID: 32859714

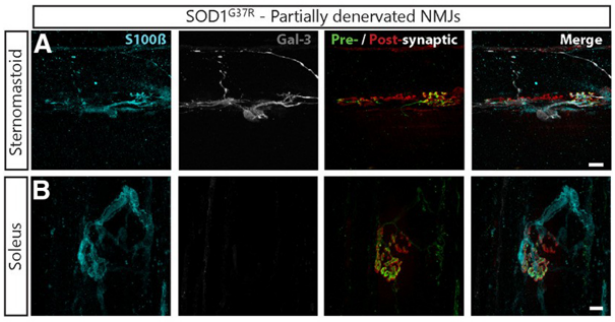

Immunofluorescence Microscopy
Gal-3 in PSCs associated with nerve terminals on partially innervated NMJs in the STM of symptomatic SOD1G37R mice. Immunolabeling of glia (blue; S100β), Gal-3 (white), and presynaptic nerve terminals and postsynaptic nAChRs (merged: respectively, green, SV2 and NF-M; red, α-BTX). A, Representative confocal images of partially innervated NMJs from the STM and (B) the SOL of symptomatic SOD1G37R mice. Note that Gal-3+-PSCs are preferentially associated with the innervated part of the endplate rather than the denervated part. Scale bars = 10 µm. PMID: 32859714

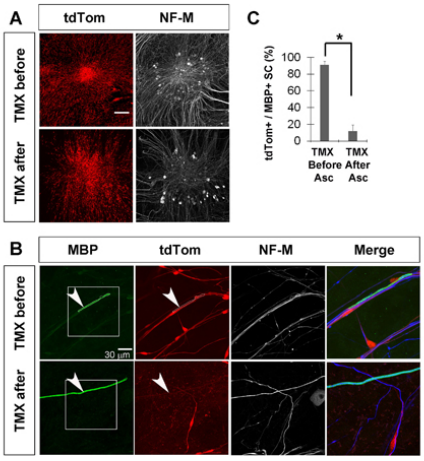

Immunofluorescence Microscopy
A, Low-magnification images of DRG explant cultures show extensive tdTom+ SC associated with DRG after addition of TMX either before or after the induction of myelination by ascorbate. B, An MBP-positive MSC (outlined in white) associated with a neurofilament-M (NF-M)-reactive neurite expresses tdTom when TMX was added before ascorbate (top row), showing that Kir4.1 was robustly expressed in this cell before myelination was induced. In contrast, neurite-associated SC failed to express tdTom when TMX was added after ascorbate, demonstrating that Cre activity in Kir4.1-CreERT2 mice was downregulated in response to myelination. C, Percentage of MBP+ Schwann cells expressing tdTom when tamoxifen was given before or after ascorbate; data in text. Expressing and non-expressing SC were defined as ones in which the tdTom fluorescence intensity within a 4 µm2 square overlapping an MBP+ region was greater than 30 or less than 20 iu8. Fig 6.
PMID: 36479906

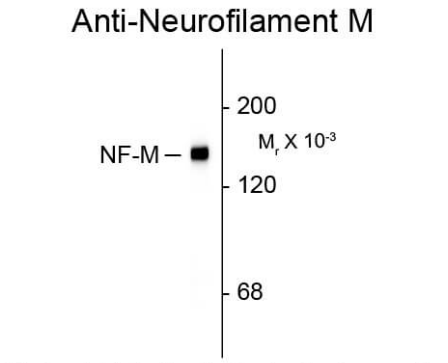

Western blot of rat cortex lysate showing specific immunolabeling of the ~145k NF-M protein.

Western Blot
Western Blot of Chicken anti-Neurofilament M antibody. Lane 1: Rat cortex lysate. Lane 2: none. Load: 20 µg per lane. Primary antibody: Neurofilament M antibody at 1:5,000 for overnight at 4°C. Secondary antibody: IRDye800™ chicken secondary antibody at 1:10,000 for 45 min at RT. Block: 5% BLOTTO overnight at 4°C. Predicted/Observed size: 145 kDa for Neurofilament M. Other band(s): none.

References

- Procacci NM et al. Kir4.1 is specifically expressed and active in non-myelinating Schwann cells. *Glia.* (2023)
- Perez-Gonzalez AP et al. Functional adaptation of glial cells at neuromuscular junctions in response to injury. *Glia.* (2022)
- Eric M. et al. Properties of Glial Cell at the Neuromuscular Junction are Incompatible with synaptic repair in the SOD1G37R ALS mouse model. *J Neurosci.* (2020)
- Martineau et al. Dynamic neuromuscular remodeling precedes motor-unit loss in a mouse model of ALS. *Elife* (2018)
- Darabid H et al. Purinergic-Dependent glial regulation of synaptic plasticity of competing terminals and synapse elimination at the neuromuscular junction. *Cell Rep.* (2018)
- Darabid H et al. Glial cells decipher synaptic competition at the mammalian neuromuscular junction. *J Neurosci.* (2013)

Disclaimer